Title
Generalizing the Discrete Gibbs Sampler-Based λ-Dynamics Approach for Multisite Sampling of Many Ligands

Journal
Journal of Chemical Theory and Computation, 17(7)

ISSN
1549-9618

Authors
Vilseck, Jonah Z
Ding, Xinqiang
Hayes, Ryan L
et al.

Publication Date
2021-07-13

DOI
10.1021/acs.jctc.1c00176

Peer reviewed

HHS Public Access

Author manuscript

J Chem Theory Comput. Author manuscript; available in PMC 2022 March 13.

Published in final edited form as:

J Chem Theory Comput. 2021 July 13; 17(7): 3895–3907. doi:10.1021/acs.jctc.1c00176.

Generalizing the Discrete Gibbs Sampler-based λ-Dynamics Approach for Multisite Sampling of Many Ligands

Jonah Z Vilseck[*,†,⊥,#], **Xinqiang Ding**[§,▯], **Ryan L. Hayes**[†], **Charles L. Brooks III**[†,‡]

[†]Department of Chemistry, University of Michigan, Ann Arbor, Michigan 48109, United States

[‡]Biophysics Program, University of Michigan, Ann Arbor, Michigan 48109, United States

[§]Department of Computational Medicine & Bioinformatics, University of Michigan, Ann Arbor, Michigan 48109, United States

[⊥]Department of Biochemistry and Molecular Biology, Indiana University School of Medicine, Indianapolis, Indiana, 46202, United States

[#]Center for Computational Biology and Bioinformatics, Indiana University School of Medicine, Indianapolis, Indiana, 46202, United States

Abstract

In this work, the discrete λ variant of the Gibbs sampler-based λ-dynamics (*d*-GSλD) method is developed to enable multiple functional group perturbations to be investigated at one or more sites of substitution off a common ligand core. The theoretical framework and special considerations for constructing discrete λ states for multisite *d*-GSλD are presented. The precision and accuracy of the *d*-GSλD method is evaluated with three test cases of increasing complexity. Specifically, methyl → methyl symmetric perturbations in water, 1,4-benzene hydration free energies, and protein-ligand binding affinities for an example HIV-1 reverse transcriptase inhibitor series are computed with *d*-GSλD. Complementary MSλD calculations were also performed to compare with *d*-GSλD's performance. Excellent agreement between *d*-GSλD and MSλD is observed, with mean unsigned errors of 0.12 and 0.22 kcal/mol for computed hydration and binding free energy test cases, respectively. Good agreement with experiment is also observed, with errors of 0.5 – 0.7 kcal/mol. These findings support the applicability of the *d*-GSλD free energy method for a variety of molecular design problems, including structure-based drug design. Finally, a discussion of *d*-GSλD versus MSλD approaches is presented to compare and contrast features of both methods.

Graphical Abstract

[*]**Corresponding Author:** jvilseck@iu.edu. Address: Department of Biochemistry and Molecular Biology, Indiana University School of Medicine, Indianapolis, Indiana, 46202, United States.

▯**Present Addresses:** Address: Department of Chemistry, Massachusetts Institute of Technology, Cambridge, Massachusetts 02139, United States.

Supporting Information. The Supporting Information is available free of charge on the ACS Publications website. The following files are available free of charge.

Additional figures and tables (PDF)

The authors declare no competing financial interest.

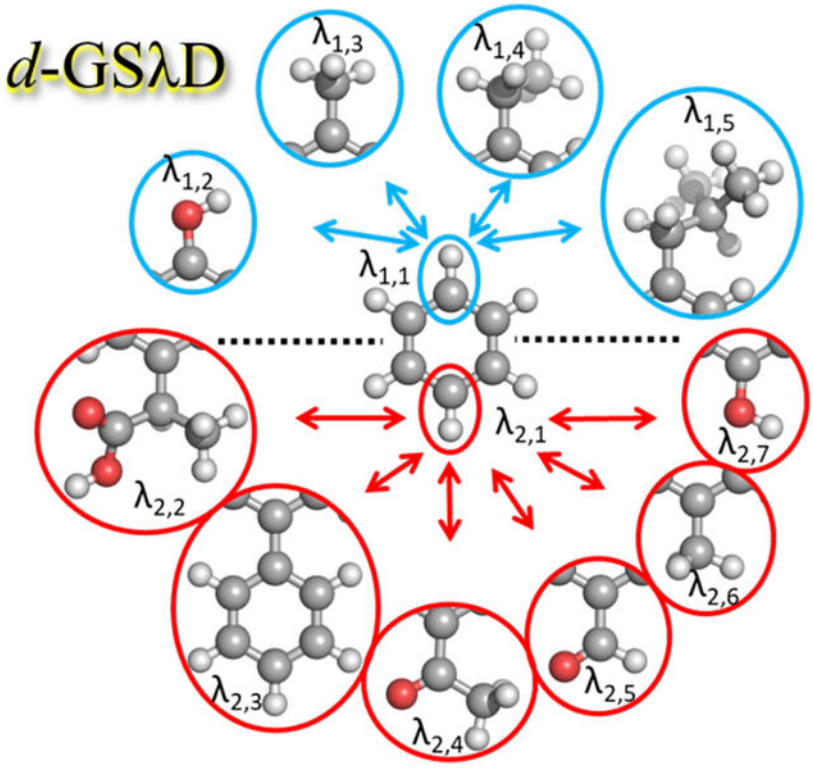

Keywords

Gibbs Sampler; λ-dynamics; free energy calculation

INTRODUCTION

With the ability to prospectively guide molecular design efforts in a variety of fields, including materials engineering and drug design, alchemical free energy calculations have become popular tools for the modern-day computational chemist.[1–7] The past few decades have seen a flurry of advancements in the field, including new methodologies,[8–14] enhanced sampling algorithms,[15–22] force field parameterization improvements,[23–30] and accelerated code implementations utilizing graphic processing units (GPUs).[31–35] Traditional free energy approaches, including free energy perturbation theory (FEP)[36] and thermodynamic integration (TI)[37], which calculate free energy differences between two thermodynamic states of a system, are still widely employed and under active development. In addition, several new methodologies have sought to break through the inherent scalability limitation associated with FEP/TI methods by calculating free energy differences between multiple thermodynamic states within a single calculation, including λ-dynamics (λD),[8,9] enveloping distribution sampling,[12,13,38] and λ-local elevation umbrella sampling (λ-LEUS) methods.[39–41]

For many years, we have been actively engaged in developing λ-dynamics-based technologies to explore combinatorial chemical spaces within a single molecular dynamics

(MD) simulation.[8,9,42] The λD-based method is especially promising for computer-aided drug design or protein engineering efforts where numerous substituents or side chain perturbations may be explored at multiple sites around a ligand or protein core.[43–48] With multisite λ-dynamics (MSλD), these many transformations can be investigated collectively and combinatorially. Not only does this facilitate a more efficient approach to explore large chemical spaces than is achievable with pairwise comparisons, but non-additive couplings between adjacent sites may also be captured. For example, recent work has shown that many tens to hundreds of combinatorial states can be successfully explored with MSλD at a fraction of the cost of running TI calculations coupled with the multistate Bennett acceptance ratio (MBAR)[11] free energy estimator.[45–48] These detailed comparative studies have demonstrated no loss of precision in the computed MSλD free energy results. Furthermore, with correct force field representations, accuracies for computed relative free energies of binding ($\Delta\Delta G_{\text{bind}}$) compared to experimental results have been good, with mean unsigned errors (MUEs) generally ranging between 0.5 – 1.0 kcal/mol.[43–48]

In the standard formulation of λD, including MSλD, the alchemical coupling parameter, λ, is treated as a continuous variable that can fluctuate dynamically between non-interacting and interacting states, 0 and 1 respectively, in a general canonical ensemble that is sampled using extended Lagrangian methods.[9,44] The inclusion of additional λ variables and appropriate implicit constraints facilitate the exploration of multiple perturbations simultaneously.[49] For a system with M sites of substitution and N_s substituents at each site, the set of all λ variables can be described as $\{\lambda\} = \{\lambda_{s,i} \mid s = 1, \ldots, M; i = 1, \ldots, N_s\}$. The potential energy of the complete system is then determined according to equation 1, and interaction energies between atoms in substituent i at site s and other environment or alchemical atoms are scaled by $\lambda_{s,i}$. In addition, multidimensional biasing potentials, $V_{bias}(\{\lambda\})$, are included to facilitate better sampling between different alchemical states in λ space.[44,46] The implicit constraints dictate that the sum of all $\lambda_{s,i}$ at each site must equal 1 $\left(\sum_{i=1}^{N_S} \lambda_{s,i} = 1\right)$, meaning that only one alchemical state of the system can exist at any given point in time. An alchemical state is defined by assigning values to each $\lambda_{s,i}$ in $\{\lambda\}$, e.g., $\{\lambda\}^A = \left\{\lambda_{s,i}^A \mid s = 1, \ldots, M; i = 1, \ldots, N_s\right\}$ for state A, to describe which site-specific substituents are interacting ($\lambda_{s,i} = 1$) with other atoms and which ones aren't ($\lambda_{s,i} = 0$). Relative free energy differences between two physical states of the system ($\Delta\Delta G(\text{A}\rightarrow\text{B})$) are then computed using the ratio of the amount of sampling of state B compared to a reference state A (equation 2).

$$V(X = (x_0, \{x\}), \{\lambda\}) = V_{env}(x_0) + \sum_{s=1}^{M} \sum_{i=1}^{N_s} \lambda_{s,i}\left(V(x_0, x_{s,i}) + V(x_{s,i})\right) + \sum_{s=1}^{M} \sum_{i=1}^{N_s} \sum_{t=s+1}^{M} \sum_{j=1}^{N_t} \lambda_{s,i}\lambda_{t,j} V(x_{s,i}, x_{t,j}) + V_{bias}(\{\lambda\}) \quad (1)$$

$$\Delta\Delta G(A \rightarrow B) \cong -k_B T ln\left(\frac{P\left(\{\lambda\}^B > \lambda_c\right)}{P\left(\{\lambda\}^A > \lambda_c\right)}\right) - \left(V_{bias}\left(\{\lambda\}^B\right) - V_{bias}\left(\{\lambda\}^A\right)\right) \quad (2)$$

In practice, the functional form of λ in MSλD prevents the $\lambda_{s,i}$ from sampling a value of exactly 0 or 1, although it may be very close, e.g., 0.9999.[49] Hence the free energy estimator uses a cutoff value (λ_c) as a threshold for the λ = 1 physical end-states (equation 2). In the most recent work employing MSλD, a cutoff of $\lambda_c > 0.99$ has been used to minimize artifacts in this finite width histogram-based estimator for determining relative free energy differences.[44–48] As a part of this work, we show that the empirical bias added to relative free energy differences computed with MSλD as a result of this histogram-based estimator is within the limits of the statistical noise and negligible when current best practices for MSλD are used.

Recently, an alternative formulation of λD was introduced that propagated λ using the Gibbs sampler framework, a Markov Chain Monte Carlo method that is well known in the field of statistical inference.[50–52] In that work, λ remained a continuous variable, but it could now exactly sample the λ = 0 and λ = 1 end-points. Highly accurate free energy estimates were then obtained with the Rao-Blackwell estimator in a similar manner as one would use MBAR to postprocess and analyze data from a TI or FEP calculation.[52–55] Applications of this continuous variant of Gibbs sampler-based λ-dynamics (*c*-GSλD) included a harmonic oscillator test system and the calculation of small molecule solvation and protein-ligand binding free energy differences. Both pairwise and triplet perturbations were explored within a single simulation. That work also introduced the idea that Gibbs sampler-based λ-dynamics (GSλD) could work with discrete λ states, rather than treating λ as a continuous variable, but the idea was not tested and fully developed.[52] We note that Chodera and Shirts also previously introduced the idea of using the Gibbs sampler framework to perform alchemical transformations with discrete λ variables and the MBAR free energy estimator; however, they mostly focused on the annihilation of a single Lennard-Jones or united-atom particle in water.[21] The GSλD framework also shares many similarities with the self-adjusted mixture sampling method introduced by Tan, except that the biases are fixed for production sampling after an initial stage of bias determination.[56,57] In this work, we develop the discrete variant of GSλD (*d*-GSλD) and demonstrate its ability to explore multiple perturbations to a chemical system simultaneously within a single MD simulation for systems with similar levels of complexity as that used in drug design. Free energy differences between all physically relevant λ end-states are then computed using FastMBAR, a recent reformulation of MBAR that is GPU enabled.[58] The validity of the new *d*-GSλD approach is evaluated through comparisons to MSλD calculations and experiment.

METHODS

Discrete Gibbs Sampler λ-Dynamics.

Gibbs sampling (GS) is well-known for its ability to sample a multidimensional distribution when direct sampling of that distribution is difficult or impossible. This is accomplished through indirect sampling of related conditional distributions, i.e., distributions that result from constraining the target distribution on a given subset of variables.[50,51] For our interest in calculating free energy differences between multiple states of a chemical system, such as between two or more ligands that have different substituents at a common point of attachment, Gibbs sampling can be performed to sample the joint distribution of atomic

coordinates, X, and alchemical states, {λ} (P(X, {λ})). As described in detail previously, GS sampling of this alchemical system can be accomplished by defining two conditional distributions, P(X|{λ}) and P({λ}|X), to sample X and {λ} iteratively while the other is constrained; sequential sampling of P(X|{λ}) and P({λ}|X) thus form a single GS step yielding X and {λ} at step t (X_t, $\{\lambda\}_t$).[52] If direct sampling of a conditional distribution is possible, numerical pseudorandom generators can be used to draw independent samples, otherwise, some other sampling technique that satisfies the condition of detailed balance with respect to the conditional distribution may be used. For example, for sampling the coordinate space of a chemical system, P(X|{λ}), traditional statistical mechanical sampling, including MD or Metropolis Monte Carlo simulations, can be used. Sampling of the {λ} space, P({λ}|X), can be accomplished directly, as described below. As long as the algorithms used to sample P(X|{λ}) and P({λ}|X) maintain conditions of detailed balance, then the sampled set of all (X_t, $\{\lambda\}_t$) configurations will converge to the desired joint distribution P(X, {λ}).[21]

In the initial formulation of GSλD, treatment of the λ coupling parameter focused on the use of a continuous variable, comparable to standard λ-dynamics based techniques, and both pairwise and multiple ligand generalizations of *c*-GSλD were presented.[52] A formulation of GSλD to work with a discrete set of λ parameters for pairwise perturbations was also discussed, with several potential advantages. First, use of discrete λ variables simplifies the conditional distribution P({λ}|X) to become a multinomial distribution that can be sampled directly using numerical methods. Second, and more importantly, the formulism of *d*-GSλD works with commonly employed soft-core potentials, or in other instances where the potential energy is nonlinearly dependent on λ, V(X, {λ}).[59,60] In contrast, use of a nonlinearly λ-dependent potential with *c*-GSλD creates a complex normalization constant in P({λ}|X), which prevents direct sampling. The flexibility provided by *d*-GSλD to use soft-core potentials is critical for applying this technique to a variety of molecular design applications while avoiding the classic singularity problem at the end-states.[59,60] This is especially relevant when an alchemical transformation accompanies a large change in volume between alchemical end-states, such as large to small functional group changes.[44] Given these advantages of the *d*-GSλD approach, this work generalizes the pairwise formulation of *d*-GSλD to investigate alchemical perturbations between multiple functional groups at one or multiple sites off a chemical core, such as a small molecule ligand.

The P(λ|X) Conditional Distribution.

To generalize *d*-GSλD to investigate multiple alchemical perturbations, equation 1 from MSλD can be used to define the joint distribution as:

$$P(X,\{\lambda\}) \propto \exp(-\beta[V_{env}(x_0) + V_{SS}(X,\{\lambda\}) + V_{MS}(X,\{\lambda\}) + G(\{\lambda\})]) \quad (3)$$

where

$$V_{SS}(X=(x_0,\{x\}),\{\lambda\}) = \sum_{s=1}^{M}\sum_{i=1}^{N_S}\lambda_{s,i}\left(V(x_0,x_{s,i}) + V(x_{s,i})\right) \quad (4)$$

$$V_{MS}(X=(x_0,\{x\}),\{\lambda\})=\sum_{S=1}^{M}\sum_{i=1}^{N_s}\sum_{t=s+1}^{M}\sum_{j=1}^{N_t}\lambda_{s,i}\lambda_{t,j}V\left(x_{s,i},x_{t,j}\right) \quad (5)$$

and $G(\{\lambda\})$ is a scalar bias added to each discrete $\{\lambda\}^i$ state to ensure equivalent sampling between different states. Analogous to MSλD, V_{SS} represents the additive interactions for all substituents at each site of transformation, and V_{MS} represents any cross-site interaction energies. The full conditional distribution P($\{\lambda\}$|X) can then be represented as a multinomial distribution:

$$P\left(\{\lambda\}^i \mid X\right)=\frac{\exp\left(-\beta\left[V_{SS}\left(X,\{\lambda\}^i\right)+V_{MS}\left(X,\{\lambda\}^i\right)+G\left(\{\lambda\}^i\right)\right]\right)}{\sum_{k=1}^{K}\exp\left(-\beta\left[V_{SS}\left(X,\{\lambda\}^k\right)+V_{MS}\left(X,\{\lambda\}^k\right)+G\left(\{\lambda\}^k\right)\right]\right.} \quad (6)$$

where K is the total number of $\{\lambda\}$ states; $G(\{\lambda\}^k)$ is the bias added to the $\{\lambda\}^k$ state. In practice, this distribution is formed by calculating the potential energy of the system at each alchemical $\{\lambda\}^i$ state and normalizing over the sum of all states to form a Boltzmann distribution. Independent samples can then be drawn from this distribution directly by selecting a new $\{\lambda\}^i$ state proportional to its probability in P($\{\lambda\}$|X) using a pseudorandom number generator. In the limiting case where only a pair of substituents are explored, i.e., M = 1 and N_s = 2, equations 3–6 simplify to the original pairwise equations introduced by Ding, *et al.*.[52]

Defining Discrete λ States.

One of the main facets associated with broadening the scope of transformations that can be explored with *d*-GSλD involves an adequate definition of the alchemical $\{\lambda\}^i$ states and the associated λ schedule between physical end-states. This is a routine consideration with FEP/TI approaches, and many papers have been published that attempt to optimize alchemical pathways or Δλ spacings between alchemical end-states.[61–65] These concerns are largely absent with MSλD or *c*-GSλD, where λ is continuous and the implicit constraints automatically control the density of sampled λ values.[9,49,52] Though it is worth noting that judicious grouping of similarly sized substituents does yield better sampling between alchemical end-states with MSλD.[43,44] With *d*-GSλD, however, one must consider how to translate a continuous λ-landscape into discrete $\{\lambda\}$ states, for which there is no unique solution. As an illustrative example, an alchemical landscape that is formed by using a continuous λ parameter for sampling five substituents at a single site may be *symbolically* represented as a continuous pentagon with vertices for each substituent (Figure 1A). In principle, for *d*-GSλD, discrete states could be defined all-throughout this same shape of chemical space (Figure 1B), but this would be inefficient and the majority of the simulation would be spent sampling non-physical intermediate $\{\lambda\}$ states. Rather, specific edges that connect end-states can be traversed (Figure 1C). This “complete” connectivity approach significantly reduces the number of discrete states needed to investigate perturbations between all of the physical end-states. It’s worth mentioning that this approach is often an ideal setup for FEP/TI calculations because closed perturbation loops can be used to reduce hysteresis in computed free energy differences;[22] but ultimately, this approach tends to be too computationally expensive to perform for routine molecular design applications with

FEP/TI methods due to the many calculations required. However, this is readily performed with λD-based methods and was the preferred choice for mapping perturbations for all *d*-GSλD calculations performed in this work. With *d*-GSλD these pathways can be explored simultaneously within a single simulation. Along each connective edge, any λ schedule may be employed. For simplicity, we used a Δλ spacing of 0.10 for constructing discrete λ states in this work. With this λ schedule, $N_S + \left[\left(\frac{N_S(N_S-1)}{2}\right)*9\right]\{\lambda\}$ states were required to sample multiple substituent perturbations at one site.

For systems where substituent perturbations are explored at more than one site, additional considerations are needed. For example, with MSλD, λ variables at two or more sites may simultaneously exist in intermediate states, $0.01 < \lambda_{s,i} < 0.99$, and concerted transitions may occur between substituents at different sites at the same time. However, attempting to generalize this continuous λ behavior with *d*-GSλD would require an appropriate λ schedule that couples alchemical changes at two or more sites. This ultimately leads to the creation of too large a number of {λ} states and makes sampling P({λ}|X) slow and inefficient due to the need to solve equation 6 for each $\{\lambda\}^i$ state. Using a large number of {λ} states also lengthens the total simulation time needed to obtain converged free energy results, since an equal amount of time should ideally be spent sampling each {λ} state and each {λ} state should be sampled several times to obtain converged free energy results. Thus, in general, the more discrete {λ} states that are used with *d*-GSλD, the more computationally expensive it becomes to run.

As an example, a set of 1,4-benzene derivatives can be considered. Using the test case described in the Computational Details section below, five substitutions at position 1 on the benzene ring (site 1) and seven additional substitutions at position 4 (site 2) can be investigated, which combinatorially yields 35 benzene states that can be sampled. Using the Δλ = 0.1 schedule described for single site perturbations only, 95 or 196 {λ} states would be required for perturbing between 5 or 7 substituents separately, respectively. Allowing for site 1 ↔ 2 transitions to occur concurrently in a *d*-GSλD simulation would thus require a total of 95 × 196 = 18,620 {λ} states. If P({λ}|X) is sampled every 100 MD steps, with a 2 fs timestep, then sampling all 18,620 {λ} states one time each would require a minimum of 3.7 ns of sampling. Instead, a balance between sampling efficiency and accuracy in computed free energy differences can be achieved by limiting concerted transitions at different sites and allowing substituent changes to occur at only one site at a time. This strategy follows precedence from previous MSλD findings for exploring large substituent modifications to a series of inhibitors bound to β-secretase 1, where it was observed that the majority of transitions between alchemical end-points, without replica-exchange enhanced sampling, occurred between substituents at the same site; simultaneous changes at both sites were rare.[47] Thus, for a two-site system with Δλ = 0.10 and allowing substituent transitions to occur only at one site at a time, reduces the number of necessary {λ} states to $(N_S \times N_t) + \left[\left(\left(\frac{N_S(N_S-1)}{2}\right)*N_t + \left(\frac{N_t(N_t-1)}{2}\right)*N_S\right)*9\right]$, where N_s and N_t refer to the number of substituents at sites s = 1 and t = 2. For the example 5 × 7 1,4-benzene system, this yields a total of 1610 {λ} states, which require only 0.32 ns of sampling to visit every {λ} state once. The total number of {λ} states have been reduced by an order of magnitude and

efficient sampling of all alchemical end-states is more readily accomplished within 10–20 ns of *d*-GSλD sampling.

d-GSλD Workflow.

A *d*-GSλD calculation begins by initializing starting values for all X and {λ} (X_0, $\{\lambda\}_0$). Similar to the procedure used for MSλD, all alchemical substituents are defined as a multiple topology model with explicit atomic coordinates, in addition to all other spectator atoms including solvent, protein, and non-alchemical ligand atoms.[43–48] Discrete {λ} states must be defined, as described previously with connective edges, such that every substituent can alchemically transform into every other substituent at each site of perturbation. After the system is energy minimized and equilibrated with a short 10 ps MD simulation, the Gibbs sampler procedure begins (Figure 2).[52] In practice, either conditional distribution may be sampled first; in this work, we chose to start with P(X|{λ}). In this regard, the coordinates of the system at step t (X_t) are generated by running a molecular dynamics simulation with a fixed $\{\lambda\}_{t-1}$ state. At the end of the MD simulation, the coordinates the system are fixed, and $\{\lambda\}_t$ is sampled. As described above, the energy of the system is calculated for every {λ} state and a Boltzmann distribution is generated. A new $\{\lambda\}_t$ is then chosen proportional to its Boltzmann probability using a pseudorandom number generator. Sequential sampling of P(X|{λ}) followed by P({λ}|X) form a single GS step (Figure 2). GS sampling is performed for a preset number of times, usually such that the total length of MD sampling performed for sampling P(X|{λ}) sums to a specific amount of time. At the conclusion of GS sampling, relative free energy differences are then computed with the FastMBAR tool by analyzing all $\{\lambda\}^i$ specific energies that were calculated on-the-fly during GS sampling.[58]

To ensure sufficient sampling is obtained, *d*-GSλD has been run in a series of 2–3 stages. The first stage involves the identification of λ biases. Like MSλD, sampling continuity between {λ} states requires those states to have similar free energies. In recent years, an automated optimization algorithm known as Adaptive Landscape Flattening (ALF) has greatly accelerated the determination of an appropriate system of biases for MSλD to flatten free energy barriers in λ-space and facilitate continuous sampling between different ligand end-states.[44,46] The use of discrete {λ} states with *d*-GSλD simplifies this system of biases into a single scalar value per {λ} state, $G(\{\lambda\}^i)$ in equation 6. In the first stage of running *d*-GSλD, these biases are identified by incorporating a Wang-Landau (WL)-like algorithm into the simulation as follows.[66,67] At the onset of the simulation, all $G(\{\lambda\}^i)$ are initialized to zero. When GS sampling commences, each $G(\{\lambda\}^i)$ is incremented by δ_{step} amount each time $\{\lambda\}^i$ is sampled. And as the simulation continues, δ_{step} decays as a function of time using the following relationship: $\delta_{step} = \frac{\delta^0}{int\left(\frac{n_{step}}{n_{delay}}\right)+1}$. In this function, n_{step} is the current GS step number and δ^0 is an initial starting δ_{step} value. The use of an *int* function allows δ_{step} to remain constant for n_{delay} steps. Though not strictly necessary, if n_{delay} equals the number of {λ} states, we've found that this facilitates slightly better sampling of all {λ} states in the early steps of WL biasing, where it is easier to get trapped in a local free energy minimum. As GS sampling continues and δ_{step} decays to values less than 1.0 kcal/mol, free energy barriers become more readily flattened across the entire λ landscape. An

important criterion for this first stage of sampling is that every {λ} state should ideally be visited several times or at a minimum once. If this is not achieved, δ^0 can be increased to larger values or the simulation can be restarted and run for longer. Next, a second shorter WL-biasing run with a $\delta^0 \leq 1.0$ kcal/mol is run to further refine and finalize the final set of $G(\{\lambda\})$ biases. Finally, after appropriate biases are obtained, production *d*-GSλD simulations can commence with fixed $G(\{\lambda\})$ biases. In this work, reported free energy results were obtained by averaging over 3–5 independent trials of full-length *d*-GSλD production simulations.

COMPUTATIONAL DETAILS

To illustrate how the *d*-GSλD method works, three test cases have been examined. First, two different symmetric methyl perturbations were investigated to ensure a $\Delta\Delta G$ of 0.00 kcal/mol was correctly obtained between all alchemical end-states. Second, free energies of hydration were computed for a variety of 1,4-benzene derivatives, consisting of 35 different end-states and 32 unique molecules.[68,69] Finally, 24 free energies of binding for indolizine containing catechol diether inhibitors targeting HIV-1 reverse transcriptase (HIV-RT) were determined.[70–72] In all test cases except the first, free energy differences were calculated with both *d*-GSλD and MSλD to evaluate elements of precision and efficiency of the new *d*-GSλD method.

All Test Systems.

All *d*-GSλD simulations were run with OpenMM using the CUDA platform.[33] Starting psf topology and pdb coordinate files were first generated with the CHARMM molecular simulation package.[73,74] CHARMM-based force field parameters were used to represent different components of the chemical systems, specifically CHARMM36 was used for all protein atoms and the MATCH atom parameterization tool was used to assign CHARMM General Force Field (CGenFF) parameters for all small molecule atoms.[29,75–79] The TIP3P water model was used to represent water.[80] Cubic, periodic solvent boxes were constructed with the *convpdb.pl* tool from the MMTSB toolset, with a 12 Å buffer between solute atoms and box edges.[81] The indolizine – HIV-RT system additionally included an appropriate number of Na^+ and Cl^- atoms to neutralize the net charge of the system and provide an ionic concentration of 0.1 M NaCl. Alchemical functional groups were created as a multiple topology model, with explicit atoms for every unique functional group. UCSF Chimera was used to build the small molecule structure files and PyMOL and VMD were used to visualize and analyze simulation trajectories.[82–84] In OpenMM, the CHARMM generated psf and pdb files were loaded in with the *CharmmPsfFile* and *CharmmParameterSet* classes. A nonbonded lookup table was generated to handle CHARMM's NBFIX nonbonded parameter exceptions, and custom nonbonded forces were written to facilitate λ scaling of all alchemical functional groups. To simplify comparisons between *d*-GSλD and MSλD free energy results, these custom nonbonded forces included CHARMM's force switching and λD-based soft-core potentials, thus matching the potentials used in CHARMM when performing MSλD calculations.[44,85]

All MSλD calculations were run with the CHARMM molecular simulation package (developmental version c44a1) utilizing the domain decomposition (DOMDEC) module to enable GPU accelerated simulations.[34,73,74] Standard MSλD procedures were followed.[43–47] In brief, each alchemical system was set up as a multiple topology model within the BLOCK module in CHARMM. This module facilitates the scaling of different functional groups by site specific λ parameters, as well as a system of biasing potentials necessary for dynamic sampling of all λ states. An implicit constraint coefficient of 5.5 was also used for all chemical systems.[49] All intramolecular interactions were treated at full strength, while all electrostatic and van der Waals interactions were scaled by λ. To avoid the classic endpoint singularity problem,[59,60] a nonbonded soft-core potential was used.[44] During MSλD sampling, λ values were saved every 10 steps for computing free energy differences according to equation 2. A cutoff value of $\lambda > 0.99$ was used for approximating end-state populations at $\lambda = 1.0$. Prior to performing production simulations, the ALF algorithm was used to identify appropriate biases for each alchemical function group.[44,46] In all test systems, iterative calculations of fifty 100 ps simulations followed by fourteen 1 ns simulations were used to identify all biasing potentials.

Similar parameters were used for running production molecular dynamics simulations in conjunction with both *d*-GSλD and MSλD. All MD simulations were performed at 25° C and 1 atm in the isothermal-isobaric ensemble. In OpenMM, this was accomplished with a Monte Carlo barostat and a Langevin integrator with a friction coefficient of 10 ps^{-1}; in CHARMM, a Langevin pressure piston with a friction coefficient of 10 ps^{-1} and a Nose-Hoover thermostat were used.[86–88] In both programs, an integration time step of 2 fs was used, facilitated by constraining all hydrogen to heavy atom bond lengths with the SHAKE algorithm.[89] Periodic boundary conditions were employed with nonbonded cutoffs of 12 Å, and force switching was used to gradually smooth nonbonded forces to zero between 10–12 Å.[85] Prior to production dynamics, each chemical system was subjected to 500–1000 steps of energy minimization at a fixed λ state, and a brief 10–30 ps of equilibration was performed to relax the system. The following sections describe more system-specific computational details, including the amount of production sampling used for each system.

Symmetric Methyl Perturbations.

Symmetric perturbations provide a useful control experiment for evaluating alchemical free energy methods. Without having to worry about force field inaccuracies, accuracy in transforming one substituent into an identical but distinct substituent replies solely on sampling proficiency and statistical rigor of the method. In addition, the expected ΔG answer of 0.00 is known, thus simplifying interpretation of the results. In this work, we first began by analyzing a toluene → toluene mutation in water, by replacing one methyl group with a different methyl group attached a benzene ring. We subsequently explored a p-xylene → p-xylene mutation in water, by replacing two para-methyl groups on a benzene ring with 2 new methyl groups at each site (a 2 × 2 multisite system). Due to the combinatorial nature of this 2-site perturbation, 4 relative free energy differences between 4 unique p-xylene end-states could be calculated from one *d*-GSλD calculation (Table 1). In both symmetric perturbations, only the methyl groups and the carbon they were bound to in the benzene ring were alchemically perturbed; all other ring atoms were treated as environment atoms. Edges

between end-states were constructed with $\Delta\lambda = 0.10$ steps, yielding a total of 11 and 40 λ states for the toluene and p-xylene perturbations, respectively. $G(\{\lambda\})$ biases were obtained with WL sampling over a single *d*-GSλD run of 100 ps using an initial $\delta^0 = 2.0$ kcal/mol and a n_{delay} equivalent to the total number of λ states for each system. No additional bias refinement was needed. Production sampling was then performed in triplicate for 1 ns of MD sampling. In the GS algorithm, sampling of $P(X|\{\lambda\})$ lasted for 100 MD steps, followed by direct sampling of $P(\{\lambda\}|X)$. At the end of the simulation, energies for each {λ} state from all triplicate production runs were collectively analyzed with FastMBAR to compute the free energy differences in water (ΔG_{water}) with respect to the first $\{\lambda\}^i$ reference state. Free energy differences were also bootstrapped with FastMBAR to determine standard deviations ($\pm \sigma$) for each ΔG_{water}.[58]

1,4-Benzene Free Energies of Hydration.

Hydration free energies, which consider an entire thermodynamic cycle of both water and gas phase calculations (Figure S1A), were investigated next for a variety of 1,4-benzene derivatives. As shown in Figure 3A, five substituents were perturbed at site 1, and an additional 7 substituents were explored at site 2, in the para position to site 1. Both small and large perturbations were considered, including the mutation of an entire phenyl ring, and substituents varied in both flexibility and polarity. The propionic acid on site 2 was modeled in its neutral form to remove any difficulties associated with charge changes between neutral and anionic substituents on the molecule. Charge changes continue to pose particular challenges for alchemical free energy calculations.[90–95] Combinatorically, 35 distinct molecules can be created from these pairings, but only 32 unique molecules exist due to some symmetry in substituents at sites 1 and 2.

For *d*-GSλD, a total of 1610 {λ} states were generated with a λ schedule of $\Delta\lambda = 0.10$ steps along connective edges between end-states, and by allowing only one site to mutate at any one time. Initial $G(\{\lambda\})$ biases were obtained over a 5 ns simulation with WL biasing. Preliminary investigations with $\delta^0 = 5.0$ or 8.0 kcal/mol failed to sample all {λ} states, including two of the end-states, within a 5 ns simulation suggesting a larger δ^0 was required. Owing to the variety of substituent sizes and properties in this system, we found that a $\delta^0 = 10.0$ kcal/mol worked well for sampling all 1610 {λ} states; n_{delay} was again set to the number of {λ} states. Refined biases were then obtained by running an additional 5 n_{delay} iterations of WL biasing, i.e., ($n_{delay} * 5$) GS steps, with a $\delta^0 = 1.0$ kcal/mol. Five independent duplicates of a 25 ns production simulation were then run with the final $G(\{\lambda\})$ biases. Energies for each {λ} state were saved every 100 MD steps, and at the end, FastMBAR was used to analyze energies from all five duplicate simulations collectively. For complementary MSλD calculations, ALF was used to determine appropriate λ biases, and five duplicate 25 ns production runs were performed. Relative free energies of hydration were calculated according to equation 2. For both *d*-GSλD and MSλD, the first 5 ns of each of the 25 ns production simulations was discarded as equilibration and excluded from the free energy analyses. To better facilitate comparisons between λD methods and to experiment, relative free energy differences were converted into absolute free energy differences using equation 7.[10,96]

$$\Delta G_{comp} = \Delta\Delta G_{comp} - \left(\frac{\sum \Delta\Delta G_{comp}}{n} - \frac{\sum \Delta G_{expt}}{n} \right) \quad (7)$$

Indolizine Inhibitor Free Energies of Binding.

To confidently use *d*-GSλD for a variety of computational investigations and in drug discovery, free energies of protein-ligand binding were next investigated. Using the thermodynamic cycle in Figure S1B, free energy differences were computed for the ligand in both unbound solvated and protein bound thermodynamic states. Following procedures used previously for modeling catechol-diether inhibitors bound to HIV-RT,[45,71,72] the protein in the complexed state of the ligand was represented in a truncated form where only residues within 20 Å of any bound ligand atom were represented. To prevent protein unfolding, all atoms of residues beyond 10 Å of any ligand atom were harmonically restrained with a force constant of 10 kcal/mol·Å^2.[97] All peptide fragments generated from truncating the full HIV-RT structure, were capped with neutral *ACE* and *CT3* CHARMM patches. The indolizine ligand was then set up with three sites of perturbations, with 3, 2, and 4 substituents respectively (Figure 3B). Sampling all perturbations collectively with λD-based approaches allows free energy differences to be computed for 24 unique molecules from a single simulation. Free energy calculations proceeded very similarly to the steps used to investigate the 1,4-benzene free energies of hydration. For *d*-GSλD, 672 {λ} states were created with Δλ = 0.10 steps along connective edges between end-states. Owing to greater similarity between alchemical substituents in this system, we postulated that $G(\{\lambda\})$ biases could be obtained from an initial simulation using a δ^0 of 4.0 kcal/mol, which successfully enabled adequate sampling of all {λ} states within a 5 ns simulation. Bias refinement then occurred via an additional run of n_{delay} * 5 GS steps with δ^0 = 1.0 kcal/mol. In both biasing runs, n_{delay} was 672. Production *d*-GSλD simulations were run for 25 ns with 5 independent duplicates, and free energy differences and standard deviations were calculated with FastMBAR. MSλD calculations were also run for 25 ns with 5 independent duplicates. For both methods, an initial segment of 5 ns was removed for equilibration prior to relative binding free energy determination, and relative free energies were converted into absolute values using equation 7.

RESULTS

Symmetric Methyl Perturbations.

Symmetric perturbations were explored in two simplistic test cases to evaluate the correctness of the *d*-GSλD approach. First, a single-site toluene → toluene transformation was evaluated by perturbing methyl group A on a benzene ring into a separate, distinct methyl group B (Table 1). After 1 ns of production sampling, a ΔG_{water} of 0.004 ± 0.020 kcal/mol was obtained, correctly matching an expected difference of 0.00 kcal/mol for symmetric perturbations. Second, a two-site p-xylene → p-xylene mutation was explored by allowing methyl groups A and C at sites 1 and 2 to mutate into B and D methyl groups, respectively. This 2 × 2 multisite system combinatorially provides access to 4 p-xylenes with A+C, A+D, B+C, and B+D group pairings. Despite using 4 times the number of lambda

states to represent all alchemical edges and intermediates in this system, compared to the toluene ⟶ toluene perturbation, 1 ns of sampling continued to provide adequate sampling of all 40 {λ} states. As shown in Figure S2, all {λ} states were frequently sampled over the course of the simulation across all three independent trials, and rapid transitions between states were accomplished. Calculated free energy differences were all less than 0.02 kcal/mol for the A+D, B+C, and B+D pairs, and all values were within statistical noise of the ideal ΔG_{water} = 0.00 kcal/mol. These results suggest that the *d*-GSλD method is working correctly and efficiently for both single-site and multisite perturbations.

1,4-Benzene Free Energies of Hydration.

Building on the success of the symmetric test systems, *d*-GSλD was next applied to computing hydration free energies (ΔG_{hyd}) for a variety of 1,4-benzene derivatives. Substituents that differed in size, flexibility, and polarity were specifically chosen to challenge the free energy method, as well as yield as large a subset of molecules as possible that could be compared to available experimental data.[68,69] The ability to explore combinatorial chemical spaces through multisite perturbations is tested through the simultaneous exploration of 5 and 7 substituents at two substitution sites. Comparable calculations were also performed with MSλD, using similar simulation parameters and potentials, to facilitate a comparison of precision and efficiency between these λD-based techniques. In previous benchmark studies, MSλD has shown excellent agreement to other free energy methods, including conventional TI/MBAR calculations, with MUEs of 0.30 – 0.50 kcal/mol, and thus serves as a viable method for comparison.[45–48]

As shown in Figure 4A, excellent agreement is observed between *d*-GSλD and MSλD methods. The raw data is reported in Table S1 of the Supporting Information. A MUE of 0.122 kcal/mol and a Pearson correlation coefficient of 0.998 were obtained. *d*-GSλD agrees within statistical noise to MSλD, confirming that this new approach is precise and accurate in comparison to other free energy methods. It is especially notable that these free energy calculations were performed in separate software packages, OpenMM and CHARMM for *d*-GSλD and MSλD respectively.

For the 19 molecules for which experimental ΔG_{hyd} are available,[68,69] good agreement between *d*-GSλD computed results and experiment was also observed (Figure 4B). We note that accuracy in this test depends both on sampling with the alchemical free energy method and correct energetic descriptions of the chemical system by the CGenFF force field. A computed MUE of 0.52 kcal/mol is good and corresponds to the expected level of accuracy that has been seen with most molecular mechanics force fields for reproducing free energies of hydration.[24,68,69,98–100] Out of these 19 molecules, only two have errors larger than 1.0 kcal/mol, acetophenone and ibuprofen, 6 molecules have errors between 0.5 – 1.0 kcal/mol, and 10 have errors less than 0.5 kcal/mol (Table S1). The high levels of precision between *d*-GSλD and MSλD and accuracy between *d*-GSλD and experiment suggest the *d*-GSλD approach is well-suited to determine condensed phase free energy differences.

Indolizine Inhibitor Free Energies of Binding.

Finally, to establish confidence in applying *d*-GSλD to problems of molecular design and drug discovery, free energies of binding were calculated for a series of indolizine containing catechol diether inhibitors bound to HIV-RT.[70,71] Mirroring simulations that have been performed previously with MSλD, 24 indolizine inhibitors were investigated with *d*-GSλD and MSλD by perturbing between 2 – 4 substituents at three sites off a central common core (Figure 3B).[45] Computed binding free energies are reported in Table S2 and graphically represented in Figure 5. In general, excellent agreement is observed between *d*-GSλD and MSλD free energy methods, with a MUE of 0.22 kcal/mol and a Pearson R of 0.97. All unsigned differences (USD) between the two λD-based results were less than 0.50 kcal/mol, except for a single $Cl/CH_3/CH_3$ ligand with a USD of 0.59 kcal/mol. Visually, there is tight correlation between free energy results over a range of 4.0 kcal/mol (Figure 5A), and the best fit line nicely correlates with the ideal y=x trend and is offset by only 0.05 kcal/mol. The uncertainties from MSλD are a little larger than with *d*-GSλD, 0.22 vs 0.09 kcal/mol respectively; however, both are considered small and within the range of typical uncertainties for computed binding free energies.[24,68,69,98–100]

Good agreement with experiment is also obtained (Figure 5B). From the set of 24 indolizine inhibitors, 11 molecules had reported experimental data for comparison.[70,71] Experimental free energies were estimated from reported EC_{50} values using this relationship: $\Delta G_{bind} = RTln(EC_{50})$, and the experimental uncertainties are unknown. The MUE between computed and experimental results is small at 0.70 kcal/mol, which agrees well with free energy benchmarks in the literature for computing protein-ligand binding affinities.[4,7,10,22,48,64,70,71,95] However, the spread of the data is greater for this analysis with a Pearson R of 0.56. As mentioned earlier, accuracy stems from complete statistical sampling as well as good force field parameters for a chosen chemical system;[101] it is also notable that the range in free energy for these molecules is small (2–2.5 kcal/mol), excluding the weakest binder. The agreement between *d*-GSλD and MSλD in both this analysis (Figure 5A), and for the 1,4-benzene ΔG_{hyd} (Figure 4A), suggests sampling is converged in both λD-based techniques. Hence, we suspect that the poorer correlation observed in Figure 5B stems mainly from force field inaccuracies. For example, a previous MSλD study of these and other fused-ring catechol diether inhibitors found that Cl atoms at the Z site (Table S2) tended to yield computed affinities that were too favorable compared to experiment.[45] This trend is again observed in this work, with Cl/CN/Cl and H/CN/Cl ligands predicted to be more favorable than experiment by 1.2–1.4 kcal/mol. Previous findings also indicated that ligands with F atoms were modeled with higher accuracies, below 0.5 kcal/mol.[45] For the 5 fluorine containing compounds in this dataset with experimental data, a MUE of 0.33 is observed, matching the previous findings. Combining observations between *d*-GSλD, MSλD, and experimental comparisons thus illustrates high precision and accuracy in *d*-GSλD computed free energies of protein-ligand binding, assuming accurate force field representations.

DISCUSSION AND CONCLUSIONS

In this work, the discrete λ variant of GSλD has been developed and expanded to explore multiple ligand perturbations at one or more sites. In accomplishing this development, *d*-GSλD joins conventional λD-based techniques in overcoming a classic scalability limitation associated with traditional FEP or TI calculations. Previous work has shown that a combinatorial exploration of chemical space is 10–20 times more efficient with MSλD than pairwise TI calculations only.[45–48] We anticipate similar efficiency gains will be observed with *d*-GSλD. For example, although comparable TI or MBAR calculations were not performed for the 1,4-benzene or indolizine inhibitor test systems, a comparable $CH_3 \rightarrow CH_3$ symmetric toluene perturbation was performed with TI/MBAR,[11,37] using identical simulation parameters and conditions as *d*-GSλD in OpenMM. A single λ window took about 2.4 mins for a 1 ns simulation; a full perturbation consisting of 11 λ windows with $\Delta\lambda = 0.10$ steps would thus require ca. 26.4 mins if all windows were run sequentially on the same GPU. In contrast, *d*-GSλD took only 10.4 mins for 1 ns of production sampling, demonstrating an efficiency gain of 2.5. Greater gains are achieved through combinatorial searches. Extrapolating the $CH_3 \rightarrow CH_3$ TI performance to the p-xylene → p-xylene system suggests a total of 79.2 mins of sequential sampling would be required to connect all four symmetric end-states. With *d*-GSλD, a 1 ns multisite simulation of all end-states required only 12.2 mins, minimally extending the time required for the toluene pairwise calculation and increasing *d*-GSλD's efficiency over TI to a factor of 6.5. For the 1,4-benzene and indolizine inhibitor test cases, which alchemically explore larger combinatorial spaces, even greater efficiency gains over TI are expected.

For example, TI calculations preformed in CHARMM from a previous MSλD study investigating indole-derivatized catechol diether inhibitors bound to HIV-RT can be used to estimate the efficiency gains of *d*-GSλD for computing ligand binding affinities.[45] In that study, 49 separate TI calculations were performed to compute 34 relative free energies of binding; redundant calculations were performed to create closed perturbation cycles. For each alchemical transformation, 11 windows of $\Delta\lambda = 0.1$ and 2.5 ns of sampling per window were used to calculate free energy differences, and transformations were performed in triplicate with different initial velocity seeds. The protein-bound simulations required approximately 3.96 hours per window to run to completion, not including the time required for post-production and MBAR analysis. For the indolizine – HIV-RT system considered in this work a minimum of 23 transformations would be required to compute relative free energy differences for all 24 indolizine end-states (compare to Table S2), not including any redundant calculations typically used to minimize free energy hysteresis around closed cycles or the extra time needed to postprocess TI trajectories prior to running MBAR. Considering the extensive similarities of system size and setup between previous-indole and current-indolizine ligand systems bound to a truncated HIV-RT model, TI calculations for the current-indolizine system would also require an estimated 3.96 hours per λ window, or 43.56 hours for a full transformation consisting of 11 λ windows. A total of 23 transformations run in triplicate would thus require 3005.64 hours of estimated wall-time, equating to 1.90 μs of total TI sampling for the protein-bound simulations only. In contrast, computing 24 $\Delta\Delta G_{bind}$ with *d*-GSλD required only 5.67 ns of sampling to determine

suitable G({λ}) biases followed by five independent 25 ns production simulations. This yielded a total amount of sampling of 130.76 ns for the *d*-GSλD protein-bound simulations, which run for ca. 226.55 hours on the same computer system. Efficiency gains of *d*-GSλD vs TI for the protein-bound simulations are thus estimated to be 13.3 or 14.5 times better for *d*-GSλD based on total run-time lengths or total MD sampling, respectively. Inclusions of the solvent-unbound ligand simulations may slightly affect these ratios, however, if identical sampling is performed for these calculations, the estimated 14.5 factor efficiency gain based on total MD sampling for *d*-GSλD over TI would remain the same.

Extensive comparisons between *d*-GSλD and MSλD were made in this work. For computed free energy differences, excellent agreement was observed between these two methods, with MUEs ranging between 0.12 – 0.22 kcal/mol. This high degree of agreement is, in part, achieved because much effort was expended to ensure that similar simulation parameters and matching potential energy equations that are routinely used with MSλD were coded into OpenMM for *d*-GSλD; thus, enabling as close to an apples-to-apples comparison as possible. A recent study, for example, has identified that significant ΔG differences may sometimes arise from differences in simulation protocols, parameters, or software packages used to perform the free energy calculations, despite looking at the same chemical system and alchemical perturbations.[102–104] This excellent agreement between *d*-GSλD and MSλD can also be attributed to the statistical rigor and correctness of the multisite *d*-GSλD approach, and adequate sampling performed thereby. This is also clearly demonstrated by the successful computation of $\Delta G_{\text{water}} = 0.0$ kcal/mol for both symmetric toluene and p-xylene test systems, within the range of statistical uncertainties.

Given the excellent agreement between *d*-GSλD and MSλD, what are the advantages to using one method over the other? For *d*-GSλD, the use of discrete {λ} states greatly simplifies the system of biases needed to run a λD simulation. Rather than fitting coefficients for several biasing potentials to flatten a multidimensional free energy landscape, as done with ALF for MSλD, *d*-GSλD can use a Wang-Landau like algorithm to determine a single, scalar bias per {λ} state.[66,67] We find that this approach required 3–4 times less sampling to obtain biases for *d*-GSλD, as compared to MSλD, which enabled production simulations to be started sooner. However, the use of discrete {λ} states can also be restrictive. For multisite systems, careful selection of which {λ} states are used with *d*-GSλD is required before any simulation can begin, and the combinatorial nature of multisite perturbations greatly increases the total number of {λ} states that are needed. For example, for the 5 × 7 1,4-benzene test system, the number of discrete {λ} states that could have been used with a $\Delta\lambda = 0.1$ ranged between ca. 1600 – 18000 possible states. Adding additional substituents would be possible, but it is likely that a 3-site system with 5 or more substituents at each site, representing 125 combinatorial end-states, would be too large to run with *d*-GSλD, at least without requiring very long simulations to converge the free energy results. With MSλD, however, worries about λ scheduling and end-state path traversal are removed with the use of continuous λ variables. Previous work has shown that with MSλD, a 3–5 site systems with up to 8 substituents at each site, amounting to 512 unique molecules, is readily accomplished.[45,46,48] Thus, MSλD can readily explore very large combinatorial chemical spaces of more than 125 alchemical end-states, while *d*-GSλD may be best suited to explore systems with fewer than 125 end-states, simultaneously within

a single simulation. Additional simulations can also be run in parallel to explore more molecules.

In our method comparisons, timing differences between *d*-GSλD and MSλD were also considered. Table S3 shows estimated wall-times for running a 1 ns simulation with each method for two of the test cases studied. In all explicit water simulations, including a protein bound simulation, MSλD was on average 2.6 times faster than *d*-GSλD's elapsed wall time. The MSλD gas phase simulation was even faster. A number of factors contribute to these differences in speed. First, the implementation of custom nonbonded forces in OpenMM is expected to be less optimal than using OpenMM's standard nonbonded forces or CHARMM's FORTRAN code that has been specifically programmed to run MSλD, though this likely contributes only a small amount to the observed performance differences. The larger contributing factor, however, stems directly from the GS routine in *d*-GSλD. To accurately sample the P({λ}|X) conditional distribution, energies from each {λ} state must be determined for all alchemical atoms scaled by λ; interaction energies between environment atoms can be ignored. For large multisite systems, this equates to hundreds of energy calculations every GS step, which will lengthen a simulation's elapsed wall time. The indolizine and 1,4-benzene systems used 672 and 1610 {λ} states, respectively, thus an equal number of energy evaluations were required every GS iteration. As a general rule, the more {λ} states used in a *d*-GSλD simulation, the longer the simulation will take. We emphasize, however, that despite this trend, significant efficiency gains over conventional FEP and TI methods are still expected with *d*-GSλD, as discussed earlier for the p-xylene test case and the HIV-RT calculations. The longer production simulation of *d*-GSλD is also, in part, counterbalanced by the ability to start sampling sooner via a faster determination of $G(\{\lambda\})$ biases.

A subtler advantage of the *d*-GSλD approach is the ability to sample all λ = 1.0 end-states explicitly. Highly accurate free energy differences can then be obtained by coupling λ- and configuration-specific energies with the FastMBAR free energy estimator.[58] It is interesting to note that the MUE's between *d*-GSλD, which exactly samples all λ = 1.0 end-states, and MSλD, which uses a histogram-based estimator, agree to within 0.1 – 0.2 kcal/mol. The level of agreement between λD approaches, run with separate software packages, suggests that artifacts introduced into the MSλD free energy results by the $\lambda_c > 0.99$ estimator are minimal. In most protein-ligand binding calculations, typical statistical uncertainties in computed free energies often range between 0.2 – 0.4 kcal/mol. Experimental uncertainties often range 0.3 – 0.5 kcal/mol, and agreement between computed and experimental free energy differences is not likely to exceed 0.4 – 0.7 kcal/mol.[10] Considering these boundaries, the differences of 0.1 – 0.2 kcal/mol can be considered within typical levels of noise and thus negligible. This study, in combination with the now many comparisons between MSλD and TI or FEP methods,[45–48] further establish the use of λD-based techniques for investigating protein-ligand binding affinities and, ultimately, drug discovery.

Use of discrete states with GS sampling is also advantageous for on-the-fly convergence checks with *d*-GSλD and FastMBAR, prior to the termination of a lengthy production simulation. As mentioned earlier, sampling the P({λ}|X) conditional distribution requires

configuration specific energies to be calculated for every {λ} state each GS step. By saving these energies to disk and periodically analyzing them with FastMBAR as a function of time, one can monitor the convergence of free energy estimates on-the-fly as the simulation progresses. For very long production simulations, this may enable simulations to be terminated when $\Delta\Delta G$s have converged, rather than at the end of a preset amount of sampling. Figures S3 and S4 show such convergence plots for the 1,4-benzene and indolizine inhibitor test cases, respectively. Over the course of *d*-GSλD sampling, and after the initial 5 ns of equilibration is removed, the computed absolute ΔGs quickly plateau after ~10 ns of sampling. The slopes from the last three data points, corresponding to the last 4 ns of sampling, average 0.0017 and −0.0038 across all 1,4-benzene and indolizine perturbations, respectively. Thus, sampling with *d*-GSλD is reasonably well converged after 20 ns of production sampling for the various multisite perturbations that were explored in this work.

To conclude, the ability to explore multiple functional group perturbations has been introduced into the proposed discrete λ variant of GSλD. Perturbations can occur at one or more sites of a common ligand core. Three test systems have confirmed the precision and accuracy of *d*-GSλD computed free energy results compared to MSλD, with MUEs of 0.1 – 0.2 kcal/mol, and compared to experiment, with MUEs of 0.5 – 0.7 kcal/mol. The use of discrete {λ} states greatly simplifies the determination of λ-specific biases for running *d*-GSλD, facilitates on-the-fly convergence checks, and allows λ = 1.0 end-states to be explicitly sampled. Highly accurate free energy estimates have been obtained using the FastMBAR free energy estimator. Like MSλD, scalability and efficiency gains over conventional TI/FEP methods are expected when using *d*-GSλD to explore multiple substituent modifications simultaneously within a single simulation. *d*GSλD should be straightforward to implement in a variety of software packages that already employ TI or FEP methods, as long as {λ} specific energies can be computed on-the-fly. As a result, we anticipate *d*-GSλD will find use in a variety of molecular design pursuits, including structure-based drug design.

Supplementary Material

Refer to Web version on PubMed Central for supplementary material.

Funding Sources

The authors gratefully acknowledge the National Institutes of Health, through grants GM037554, GM130587, and GM107233, for financial support.

ABBREVIATIONS

λD	λ-dynamics
MSλD	multisite λ-dynamics
GSλD	Gibbs sampler-based λ-dynamics
***c*-GSλD**	continuous variant Gibbs sampler-based λ-dynamics

***d*-GSλD**	discrete variant Gibbs sampler-based λ-dynamics
GS	Gibbs sampling
ALF	Adaptive Landscape Flattening
FEP	free energy perturbation
TI	thermodynamic integration
MD	molecular dynamics
MBAR	multistate Bennett acceptance ratio
WL	Wang-Landau
HIV-RT	HIV-1 reverse transcriptase
GPU	graphic processing unit
MUE	mean unsigned error
USD	unsigned difference
CGenFF	CHARMM General Force Field

REFERENCES

1. Kollman P Free Energy Calculations: Applications to Chemical and Biochemical Phenomena. Chem. Rev 1993, 93, 2395–2417.
2. Jorgensen WL The Many Roles of Computation in Drug Discovery. Science 2004, 303, 1813–1818. [PubMed: 15031495]
3. Song LF; Merz KM Jr. Evolution of Alchemical Free Energy Methods in Drug Discovery. J. Chem. Inf. Model 2020, 60, 5308–5318. [PubMed: 32818371]
4. Chodera JD; Mobley DL; Shirts MR; Dixon RW; Branson K; Pande VS Alchemical Free Energy Methods for Drug Discovery: Progress and Challenges. Curr. Opin. Struct. Biol 2011, 21, 150–160. [PubMed: 21349700]
5. Chipot C Frontiers in Free-Energy Calculations of Biological Systems. WIREs Comput. Mol. Sci 2014, 4,71–89.
6. Hansen N; van Gunsteren WF Practical Aspects of Free-Energy Calculations: A Review. J. Chem. Theory Comput 2014, 10, 2632–2647. [PubMed: 26586503]
7. Cournia Z; Allen B; Sherman W Relative Binding Free Energy Calculations in Drug Discovery: Recent Advances and Practical Considerations. J. Chem. Inf. Model 2017, 57, 2911–2937. [PubMed: 29243483]
8. Kong X; Brooks CL III λ Dynamics: A New Approach to Free Energy Calculations. J. Chem. Phys 1996, 105, 2414–2423.
9. Knight JL; Brooks CL III Multisite λ Dynamics for Simulated Structure-Activity Relationship Studies. J. Chem. Theory Comput 2011, 7, 2728–2739. [PubMed: 22125476]
10. Wang L; Wu Y; Deng Y; Kim B; Pierce L; Krilov G; Lupyan D; Robinson S; Dahlgren MK; Greenwood J; et al. Accurate and Reliable Prediction of Relative Ligand Binding Potency in Prospective Drug Discovery by Way of a Modern Free-Energy Calculation Protocol and Force Field. J. Am. Chem. Soc 2015, 137, 2695–2703. [PubMed: 25625324]
11. Shirts MR; Chodera JD Statistically Optimal Analysis of Samples from Multiple Equilibrium States. J. Chem. Phys 2008, 129, 124105. [PubMed: 19045004]

12. Christ CD; van Gunsteren WF Enveloping distribution sampling: A method to calculate free energy differences from a single simulation. J. Chem. Phys 2007, 126, 184110. [PubMed: 17508795]
13. Christ CD; van Gunsteren WF Simple, Efficient, and Reliable Computation of Multiple Free Energy Differences from a Single Simulation: A Reference Hamiltonian Parameter Update Scheme for Enveloping Distribution Sampling (EDS). J. Chem. Theory Comput 2009, 5, 276–286. [PubMed: 26610104]
14. Hahn DF; Hünenberger PH Alchemical Free-Energy Calculations by Multple-Replica λ-Dynamcs: The Conveyor Belt Thermodynamic Integration Scheme. J. Chem. Theory Comput 2019, 15, 2392–2419. [PubMed: 30821973]
15. Sugita Y; Kitao A; Okamoto Y Multidimensional replica-exchange method for free-energy calculations. J. Chem. Phys 2000, 113, 6042–6051.
16. Woods CJ; Essex JW; King MA The Development of Replica-Exchange-Based Free-Energy Methods. J. Phys. Chem. B 2003, 107, 13703–13710.
17. Liu P; Kim B; Friesner RA; Berne BJ Replica Exchange with Solute Tempering: A Method for Sampling Biological Systems in Explicit Water. Proc. Natl. Acad. Sci. U. S. A 2005, 102, 13749–13754. [PubMed: 16172406]
18. Fajer M; Hamelberg D; McCammon JA Replica-Exchange Accelerated Molecular Dynamics (REXAMD) Applied to Thermodynamic Integration. J. Chem. Theory Comput 2008, 4, 1565–1569. [PubMed: 19461870]
19. Jiang W; Roux B Free Energy Perturbation Hamiltonian Replica-Exchnge Molecular Dynamics (FEP/H-REMD) for Absolute Ligand Binding Free Energy Calculations. J. Chem. Theory Comput 2010, 6, 2559–2565. [PubMed: 21857813]
20. Meng Y; Sabri Dashti D; Roitberg AE Computing Alchemical Free Energy Differences with Hamiltonian Replica Exchange Molecule Dynamics (H-REMD) Simulations. J. Chem. Theory Comput 2011, 7, 2721–2727. [PubMed: 22125475]
21. Chodera JD; Shirts MR Replica exchange and expanded ensemble simulations as Gibbs sampling: Simple improvements for enhanced mixing. J. Chem. Phys 2011, 135, 194110. [PubMed: 22112069]
22. Wang L; Deng Y; Knight JL; Wu Y; Kim B; Sherman W; Shelley JC; Lin T; Abel R Modeling Local Structural Rearrangements Using FEP/REST: Application to Relative Binding Affinity Predictions of CDK2 Inhibitors. J. Chem. Theory Comput 2013, 9, 1282–1293. [PubMed: 26588769]
23. Robertson MJ; Tirado-Rives J; Jorgensen WL Improved Peptide and Protein Torsional Energetics with the OPLS-AA Force Field. J. Chem. Theory Comput 2015, 11, 3499–3509. [PubMed: 26190950]
24. Dodda LS; Vilseck JZ; Tirado-Rives J; Jorgensen WL 1.14*CM1A-LBCC: Localized Bond-Charge Corrected CM1A Charges for Condensed-Phase Simulations. J. Phys. Chem. B 2017, 121, 3864–3870. [PubMed: 28224794]
25. Wang J; Wolf RM; Caldwell JW; Kollman PA; Case DA Development and testing of a general amber force field. J. Comp. Chem 2004, 25, 1157–1174. [PubMed: 15116359]
26. He X; Man VH; Yang W; Lee T-S; Wang J A fast and high-quality charge model for the next generation general AMBER force field. J. Chem. Phys 2020, 153, 114502. [PubMed: 32962378]
27. Mobley DL; Bannan CC; Rizzi A; Bayly CI; Chodera JD; Lim VT; Lim NM; Beauchamp KA; Slochower DR; Shirts MR; Gilson MK; Eastman PK Escaping atom types in force fields using direct chemical perception. J. Chem. Theory Comput 2018, 14, 6076–6092. [PubMed: 30351006]
28. Qiu Y; Smith DGA; Boothroyd S; Jang H; Wagner J; Bannan CC; Gokey T; Lim VT; Stern CD; Rizzi A; Lucas X; Tjanaka B; Shirts MR; Gilson MK; Chodera JD; Bayly CI; Mobley DL; Wang L-P Development and Benchmarking of Open Force Field v1.0.0, the Parsley small molecule force field. ChemRxiv. Preprint. 10.26434/chemrxiv.13082561.v1.
29. Vanommeslaeghe K; Hatcher E; Acharya C; Kundu S; Zhong S; Shim J; Darian E; Guvench O; Lopes P; Vorobyov I; MacKerell AD Jr. CHARMM General Force Field: A Force Field for Drug-Like Molecules Compatible with the CHARMM All-Atom Additive Biological Force Fields. J. Comput. Chem 2010, 31, 671–690. [PubMed: 19575467]

30. Harder E; Damm W; Maple J; Wu C; Reboul M; Xiang JY; Wang L; Lupyan D; Dahlgren MK; Knight JL; Kaus JW; Cerutti DS; Krilov G; Jorgensen WL; Abel R; Friesner RA OPLS3: A Force Field Providing Broad Coverage of Drug-like Small Molecules and Proteins. J. Chem. Theory Comput 2016, 12, 281–296. [PubMed: 26584231]

31. Chen H; Maia JDC; Radak BK; Hardy DJ; Cai W; Chipot C; Tajkhorshid E Boosting Free-Energy Perturbation Calculations with GPU-Accelerated NAMD. J. Chem. Inf. Model 2020, 60, 5301–5307. [PubMed: 32805108]

32. Lee T-S; Cerutti DS; Mermelstein D; Lin C; LeGrand S; Giese TJ; Roitberg A; Case DA; Walker RC; York DM GPU-Accelerated Molecular Dynamics and Free Energy Methods in Amber18: Performance Enhancements and New Features. J. Chem. Inf. Model 2018, 58, 2043–2050. [PubMed: 30199633]

33. Eastman P; Swails J; Chodera JD; McGibbon RT; Zhao Y; Beauchamp KA; Wang L-P; Simmonett AC; Harrigan MP; Stern CD; Wiewiora RP; Brooks BR; Pande VS OpenMM 7: Rapid development of high performance algorithms for molecular dynamics. PLoS Comput. Biol 2017, 13, e1005659. [PubMed: 28746339]

34. Hynninen AP; Crowley MF New Faster CHARMM Molecular Dynamics Engine. J. Comput. Chem 2014, 35, 406–413. [PubMed: 24302199]

35. Kutzner C; Pall S; Fechner M; Esztermann A; de Groot BL; Grubmueller H More bang for your buck: Improved use of GPU nodes for GROMACS 2018. J. Comp. Chem 2019, 40, 2418–2431. [PubMed: 31260119]

36. Zwanzig RW High-Temperature Equation of State by a Perturbation Method. I. Nonpolar Gases. J. Chem. Phys 1954, 22, 1420–1426.

37. Kirkwood JG Statistical Mechanics of Fluid Mixtures. J. Chem. Phys 1935, 3, 300–313.

38. Perthold JW; Oostenbrink C Accelerated Enveloping Distribution Sampling: Enabling Sampling of Multiple End States while Preserving Local Energy Minima. J. Phys Chem. B 2018, 122, 5030–5037. [PubMed: 29669415]

39. Bieler NS; Häuselmann R; Hünenberger PH Local Elevation Umbrella Sampling Applied to the Calculation of Alchemical Free-Energy Changes via λ-Dynamics: the λ-LEUS Scheme. J. Chem. Theory Comput 2014, 10, 3006–3022. [PubMed: 26588272]

40. Bieler NS; Hünenberger PH Communication: Estimating the initial biasing potential for λ-local-elevation umbrella-sampling (λ-LEUS) simulations via slow growth. J. Chem. Phys 2014, 141, 201101. [PubMed: 25429926]

41. Bieler NS; Tschopp JP; Hünenberger PH Multistate λ-Local-Elevation Umbrella-Sampling (MS-λ-LEUS): Method and Application to the Complexation of Cations by Crown Ethers. J. Chem. Theory Comput 2015, 11, 2575–2588. [PubMed: 26575556]

42. Knight JL; Brooks CL III λ Dynamics Free Energy Simulation Methods. J. Comput. Chem 2009, 30, 1692–1700. [PubMed: 19421993]

43. Armacost KA; Goh GB; Brooks CL III Biasing Potential Replica Exchange Multisite λ Dynamics for Efficient Free Energy Calculations. J. Chem. Theory Comput 2015, 11, 1267–1277. [PubMed: 26579773]

44. Hayes RL; Armacost KA; Vilseck JZ; Brooks CL III Adaptive Landscape Flattening Accelerates Sampling of Alchemical Space in Multisite λ Dynamics. J. Phys. Chem. B 2017, 121, 3626–3635. [PubMed: 28112940]

45. Vilseck JZ; Armacost KA; Hayes RL Goh GB; Brooks CL III Predicting Binding Free Energies in a Large Combinatorial Chemical Space Using Multisite λ Dynamics. J. Phys. Chem. Lett 2018, 9, 3328–3332. [PubMed: 29847134]

46. Hayes RL; Vilseck JZ; Brooks CL III Approaching protein design with multisite λ dynamics: Accurate and scalable mutational folding free energies in T4 lysozyme. Protein Sci. 2018, 27, 1910–1922. [PubMed: 30175503]

47. Vilseck JZ; Sohail N; Hayes RL; Brooks CL III Overcoming Challenging Substituent Perturbations with Multisite λ-Dynamics: A Case Study Targeting β-Secretase 1. J. Phys. Chem. Lett 2019, 10, 4875–4880. [PubMed: 31386370]

48. Prabhu RE; Paul TJ; Hayes RL; Brooks CL III Automated, Accurate, and Scalable Relative Protein-Ligand Binding Free-Energy Calculations Using Lambda Dynamics. J. Chem. Theory Comput 2020, 16, 7895–7914. [PubMed: 33201701]
49. Knight JL; Brooks CL III Applying Efficient Implicit Constraints in Alchemical Free Energy Simulations. J. Comput. Chem 2011, 32, 3423–3432. [PubMed: 21919014]
50. Geman S; Geman D; Stochastic Relaxation, Gibbs Distributions, and the Bayesian Restoration of Images. IEEE Trans. Pattern Anal. Mach. Intell 1984, PAMI-6, 721–741.
51. Smith AF; Roberts GO Bayesian computation via the Gibbs sampler and related Markov chain Monte Carlo methods. J. R. Stat. Soc. B 1993, 55, 3–23.
52. Ding X; Vilseck JZ; Hayes RL; Brooks CL III Gibbs Sampler-Based λ-Dynamics and Rao-Blackwell Estimator for Alchemical Free Energy Calculation. J. Chem. Theory Comput 2017, 13, 2501–2510. [PubMed: 28510433]
53. Rao CR Information and accuracy attainable in the estimation of statical parameters. Bull. Calcutta Math. Soc 1945, 37, 81–91.
54. Blackwell D Conditional expectation and unbiased sequential estimation. Ann. Math. Stat 1947, 18, 105–110.
55. Gelfand AE; Smith AF Sampling-based approaches to calculating marginal densities. J. Am. Stat. Assoc 1990, 85, 398–409.
56. Tan Z Optimally Adjusted Mixture Sampling and Locally Weighted Histogram Analysis. Journal of Computational and Graphical Statistics 2017, 26, 54–65.
57. Carlson DE; Stinson P; Pakman A; Paninski L Partition Functions from Rao-Blackwellized Tempered Sampling. Proceedings of the 33rd International Conference on Machine Learning, New York, NY, USA; JMLR: W&CP, volume 48, 2016.
58. Ding X; Vilseck JZ; Brooks CL III Fast Solver for Large Scale Multistate Bennett Acceptance Ratio Equations. J. Chem. Theory Comput 2019, 15, 799–802. [PubMed: 30689377]
59. Zacharias M; Straatsma TP; McCammon JA Separation-shifted scaling, a new scaling method for Lennard-Jones interactions in thermodynamic integration. J. Chem. Phys 1994, 100, 9025–9031.
60. Beutler TC; Mark AE; van Schaik RC; Gerber PR; van Gunsteren WF Avoiding singularities and numerical instabilities in free energy calculations based on molecular simulations. Chem. Phys. Lett 1994, 222, 529–539.
61. Pohorille A; Jarzynski C; Chipot C Good Practices in Free-Energy Calculations. J. Phys. Chem. B 2010, 114, 10235–10253. [PubMed: 20701361]
62. Liu S; Wu Y; Lin T; Abel R; Redmann JP; Summa CM; Jaber VR; Lim NM; Mobley DL Lead optimization mapper: automating free energy calculations for lead optimization. J. Comput.-Aided Mol. Des 2013, 27, 755–770. [PubMed: 24072356]
63. Yang Q; Burchett W; Steeno GS; Liu S; Yang M; Mobley DL; Hou X Optimal designs for pairwise calculation: An application to free energy perturbation in minimizing prediction variability. J. Comp. Chem 2020, 41, 247–257. [PubMed: 31721260]
64. Kuhn M; Firth-Clark S; Tosco P; Mey ASFS; Mackey M; Michel J Assessment of Binding Affinity via Alchemical Free-Energy Calculations. J. Chem. Inf. Model 2020, 60, 3120–3130. [PubMed: 32437145]
65. Xu H Optimal Measurement Network of Pairwise Differences. J. Chem. Inf. Model 2019, 59, 4720–4728. [PubMed: 31613620]
66. Wang F; Landau DP Efficient, Multiple-Range Random Walk Algorithm to Calculate the Density of States. Phys. Rev. Lett 2001, 86, 2050–2053. [PubMed: 11289852]
67. Belardinelli RE; Pereyra VD Wang-Landau algorithm: A theoretical analysis of the saturation of the error. J. Chem. Phys 2007, 127, 184105. [PubMed: 18020628]
68. Mobley DL; Guthrie JP FreeSolv: a database of experimental and calculated hydration free energies, with input files. J. Comput.-Aided Mol. Des 2014, 28, 711–720. [PubMed: 24928188]
69. Matos GDR; Kyu DY; Loeffler HH; Chodera JD; Shirts MR; Mobley DL Approaches for Calculating Solvation Free Energies and Enthalpies Demonstrated with an Update of the FreeSolv Database. J. Chem. Eng. Data 2017, 62, 1559–1569. [PubMed: 29056756]

70. Jorgensen WL Computer-Aided Discovery of Anti-HIV Agents. Bioorg. Med. Chem 2016, 24, 4768–4778. [PubMed: 27485603]
71. Lee W-G; Gallardo-Macias R; Frey KM; Spasov KA; Bollini M; Anderson KS; Jorgensen WL Picomolar Inhibitors of HIV Reverse Transcriptase Featuring Bicyclic Replacement of a Cyanovinylphenyl Group. J. Am. Chem. Soc 2013, 135, 16705–16713. [PubMed: 24151856]
72. Lee W-G; Frey KM; Gallardo-Macias R; Spasov KA; Bollini M; Anderson KS; Jorgensen WL Picomolar Inhibitors of HIV-1 Reverse Transcriptase: Design and Crystallography of Naphthyl Phenyl Ethers. ACS Med. Chem. Lett 2014, 5, 1259–1262. [PubMed: 25408842]
73. Brooks BR; Brooks CL III; MacKerell AD Jr; Nilsson L; Petrella RJ; Roux B; Won Y; Archontis G; Bartels C; Boresch S; Caflisch A; Caves L; Cui Q; Dinner AR; Feig M; Fischer S; Gao J; Hodoscek M; Im W; Kuczera K; Lazaridis T; Ma J; Ovchinnikov V; Paci E; Pastor RW; Post CB; Pu JZ; Schaefer M; Tidor B; Venable RM; Woodcock HL; Wu X; Yang W; York DM; Karplus M CHARMM: The Biomolecular Simulation Program. J. Comput. Chem 2009, 30, 1545–1614. [PubMed: 19444816]
74. Brooks BR; Bruccoleri RE; Olafson BD; States BD; Swaminathan S; Karplus M CHARMM: A Program for Macromolecular Energy, Minimization, and Dynamics Calculations. J. Comput. Chem 1983, 4, 187–217.
75. Best RB; Mittal J; Feig M; MacKerell AD Jr. Inclusion of Many-Body Effects in the Additive CHARMM Protein CMAP Potential Results in Enhanced Cooperativity of α-Helix And β-Hairpin Formation. Biophys. J 2012, 103, 1045–1051. [PubMed: 23009854]
76. Best RB; Zhu X; Shim J; Lopes PEM; Mittal J; Feig M; MacKerell AD Jr. Optimization of the Additive CHARMM All-Atom Protein Force Field Targeting Improved Sampling of the Backbone ϕ, ψ, and Side-Chain χ_1 and χ_2 Dihedral Angles. J. Chem. Theory Comput 2012, 8, 3257–3273. [PubMed: 23341755]
77. Vanommeslaeghe K; MacKerell AD Jr. Automation of the CHARMM General Force Field (CGenFF) I: Bond Perception and Atom Typing. J. Chem. Inf. Model 2012, 52, 3144–3154. [PubMed: 23146088]
78. Vanommeslaeghe K; Raman EP; MacKerell AD Jr. Automation of the CHARMM General Force Field (CGenFF) II: Assignment of Bonded Parameters and Partial Atomic Charges. J. Chem. Inf. Model 2012, 52, 3155–3168. [PubMed: 23145473]
79. Yesselman JD; Price DJ; Knight JL; Brooks CL III MATCH: An Atom-Typing Toolset for Molecular Mechanics Force Fields. J. Comput. Chem 2012, 33, 189–202. [PubMed: 22042689]
80. Jorgensen WL; Chandrasekhar J; Madura JD; Impey RW; Klein ML Comparison of Simple Potential Functions for Simulating Liquid Water. J. Chem. Phys 1983, 79, 926–935.
81. Feig M; Karanicolas J; Brooks CL III MMTSB Tool Set: Enhanced Sampling and Multiscale Modeling Methods for Applications in Structural Biology. J. Mol. Graph. Model 2004, 22, 377–395. [PubMed: 15099834]
82. Pettersen EF; Goddard TD; Huang CC; Couch GS; Greenblatt DM; Meng EC; Ferrin TE UCSF Chimera--a visualization system for exploratory research and analysis. J. Comput. Chem 2004, 25, 1605–1612. [PubMed: 15264254]
83. The PyMOL Molecular Graphics System, Version 1.8, Schrodinger LLC, New York, New York, United States.
84. Humphrey W; Dalke A; Schulten K VMD – Visual Molecular Dynamics. J. Molec. Graphics 1996, 14, 33–38.
85. Steinbach PJ; Brooks BR New Spherical-Cutoff Methods for Long-Range Forces in Macromolecular Simulation. J. Comp. Chem 1994, 15, 667–683.
86. Feller SE; Zhang Y; Pastor RW; Brooks BR Constant pressure molecular dynamics simulation: The Langevin piston method. J. Chem. Phys 1995, 103, 4613–4621.
87. Nosé S A unified formulation of the constant temperature molecular dynamics methods. J. Chem. Phys 1984, 81, 511–519.
88. Hoover WG Canonical dynamics: Equilibrium phase-space distributions. Phys. Review A 1985, 31, 1695–1697.

89. Ryckaert JP; Ciccotti G; Berendsen HJC Numerical Integration of the Cartesian Equations of Motion of a System with Constraints: Molecular Dynamics of n-Alkanes. J. Comput. Phys 1977, 23, 327–341.

90. Rocklin GJ; Mobley DL; Dill KA; Hünenberger PH Calculating the binding free energies of charged species based on explicit-solvent simulations employing lattice-sum methods: An accurate correction scheme for electrostatic finite-size effects. J. Chem. Phys 2013, 139, 184103. [PubMed: 24320250]

91. Reif MM; Oostenbrink C Net charge changes in the calculation of relative ligand-binding free energies via classical atomistic molecular dynamics simulation. J. Comp. Chem 2014, 35, 227–243. [PubMed: 24249099]

92. Öhlknecht C; Lier B; Petrov D; Fuchs J; Oostenbrink C Correcting electrostatic artifacts due to net-charge changes in the calculation of ligand binding free energies. J. Comp. Chem 2020, 41, 986–999. [PubMed: 31930547]

93. Huggins D An Approach to Alchemical Binding Free-Energy Calculations Using Coupled Topologies. ChemRxiv. Preprint. 10.26434/chemrxiv.7203362.v1.

94. Chen W; Deng Y; Russell E; Wu Y; Abel R; Wang L Accurate Calculation of Relative Binding Free Energies between Ligands with Different Net Charges. J. Chem. Theory Comput 2018, 14, 6346–6358. [PubMed: 30375870]

95. Schindler CEM; Baumann H; Blum A; Böse D; Buchstaller H-P; Burgdorf L; Cappel D; Chekler E; Czodrowski P; Dorsch D; et al. Large-Scale Assessment of Binding Free Energy Calculations in Active Drug Discovery Projects. J. Chem. Inf. Model 2020, 60, 5457–5474. [PubMed: 32813975]

96. Keränen H; Pérez-Benito L; Ciordia M; Delgado F; Steinbrecher TB; Oehlrich D; van Vlijmen HWT; Trabanco AA; Tresadern G Acylguanidine Beta Secretase 1 Inhibitors: A Combined Experimental and Free Energy Perturbation Study. J. Chem. Theory Comput 2017, 13, 1439–1453. [PubMed: 28103438]

97. Brooks CL III; Brünger A; Karplus M Active site dynamics in protein molecules: A stochastic boundary molecular-dynamics approach. Biopolymer 1985, 24, 843–865.

98. Mobley DL; Bayly CI; Cooper MD; Shirts MR; Kill KA Small molecule hydration free energies in explicit solvent: An extensive test of fixed-charge atomistic simulations. J. Chem. Theory Comput 2009, 10, 350–358.

99. Shivakumar D; Deng Y; Roux B Computations of Absolute Solvation Free Energies of Small Molecules Using Explicit and Implicit Solvent Model. J. Chem. Theory Comput 2009, 5, 919–930. [PubMed: 26609601]

100. Shivakumar D; Williams J; Wu Y; Damm W; Shelley J; Sherman W Prediction of Absolute Solvation Free Energies using Molecular Dynamics Free Energy Perturbation and the OPLS Force Field. J. Chem. Theory Comput 2010, 6, 1509–1519. [PubMed: 26615687]

101. Mobley DL Let's get honest about sampling. J. Comput.-Aided Mol. Des 2012, 26, 93–95. [PubMed: 22113833]

102. Loeffler HH; Bosisio S; Matos GDR; Suh D; Roux D; Mobley DL; Michel J Reproducibility of Free Energy Calculations across Different Molecular Simulation Software Packages. J. Chem. Theory Comput 2018, 14, 5567–5582. [PubMed: 30289712]

103. Fass J; Sivak DA; Crooks GE; Beauchamp KA; Leimkuhler B; Chodera JD Quantifying Configuration-Sampling Error in Langevin Simulations of Complex Molecular Systems. Entropy 2018, 20, 318. [PubMed: 30393452]

104. Shirts MR Simple Quantitative Tests to Validate Sampling from Thermodynamic Ensembles. J. Chem. Theory Comput 2013, 9, 909–926. [PubMed: 26588735]

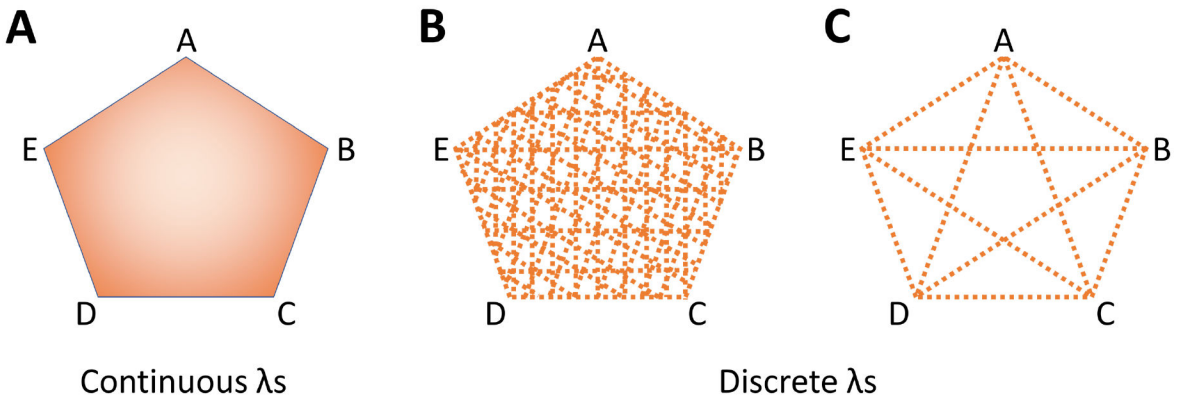

Figure 1.

Illustrations of continuous and discrete {λ} states when investigating transformations between five alchemical end-states (labeled A–E) for a hypothetical chemical system. (A) Exploration of a continuous λ surface is possible when using MSλD or c-GSλD. (B) One example discretization of the continuous λ surface in (A) into many discrete {λ} states, including all intermediary spaces between end-states. (C) Discrete {λ} states defined along edges that connect the five alchemical end-states in a pairwise manner. This significantly reduces the number of discrete {λ} states needed to explore all molecular transformations.

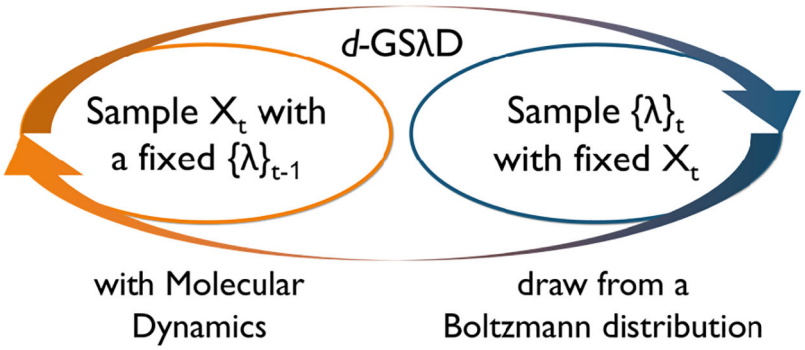

Figure 2.

The Gibbs sampler procedure used to sample the joint distribution, (P(X, {λ})), of atomic coordinates, X, and alchemical states, {λ}. Two conditional distributions, P(X|{λ}) and P({λ}|X), are iteratively sampled at time t. One complete cycle represents a single GS step in P(X, {λ}).

A

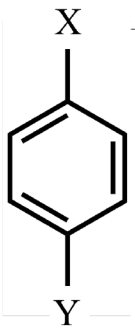

Site 1 (X)	Site 2 (Y)
H	H
OH	OH
CH_3	CH_3
ethyl	CHO
iso-butyl	$COCH_3$
	C_6H_5
	$CH(CH_3)COOH$

B

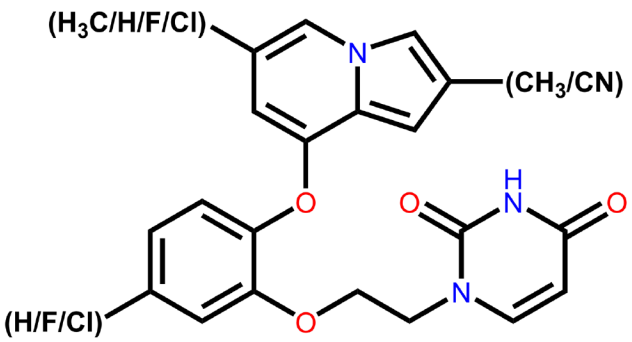

Figure 3.

(A) The 1,4-benzene derivatives investigated with λD-based free energy calculations. Five and seven substituent modifications were explored at two sites, respectively. Substituents varied in size, flexibility, and polarity. (B) Indolizine-based inhibitors bound to HIV-RT. Three sites of functional group substitutions were investigated simultaneously. Substituents that were explored are highlighted in the parentheses.

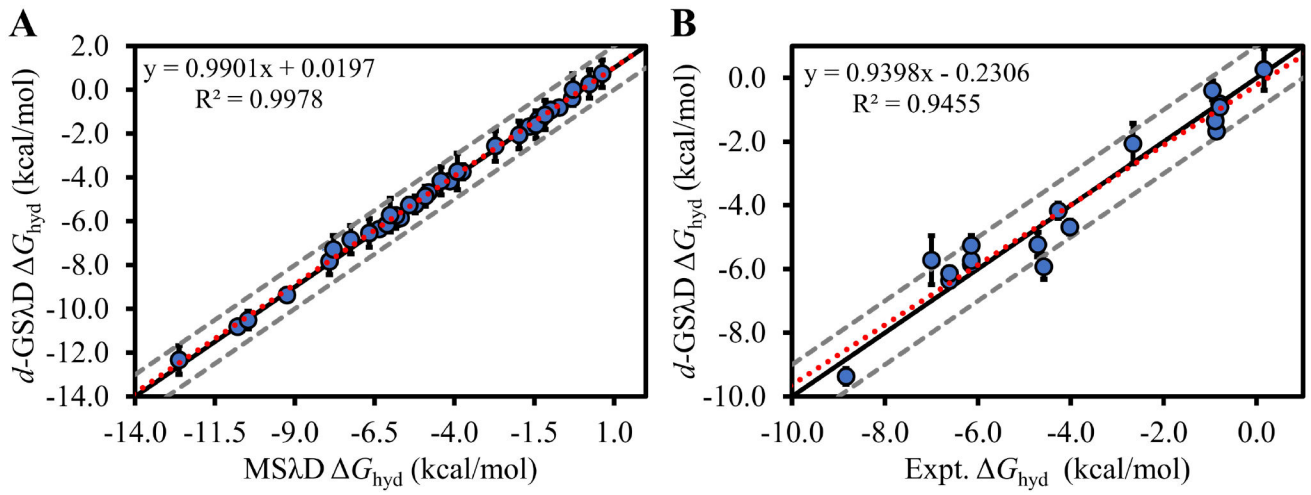

Figure 4.

(A) Correlation in computed hydration free energies (kcal/mol) between *d*-GSλD and MSλD free energy methods for 1,4-benzene derivatives. (B) Correlation in computed *d*-GSλD and experimental hydration free energies (kcal/mol). The solid black line represents y = x; dashed grey lines represent y = x ± 1. The red dotted line represents the best fit line of the data.

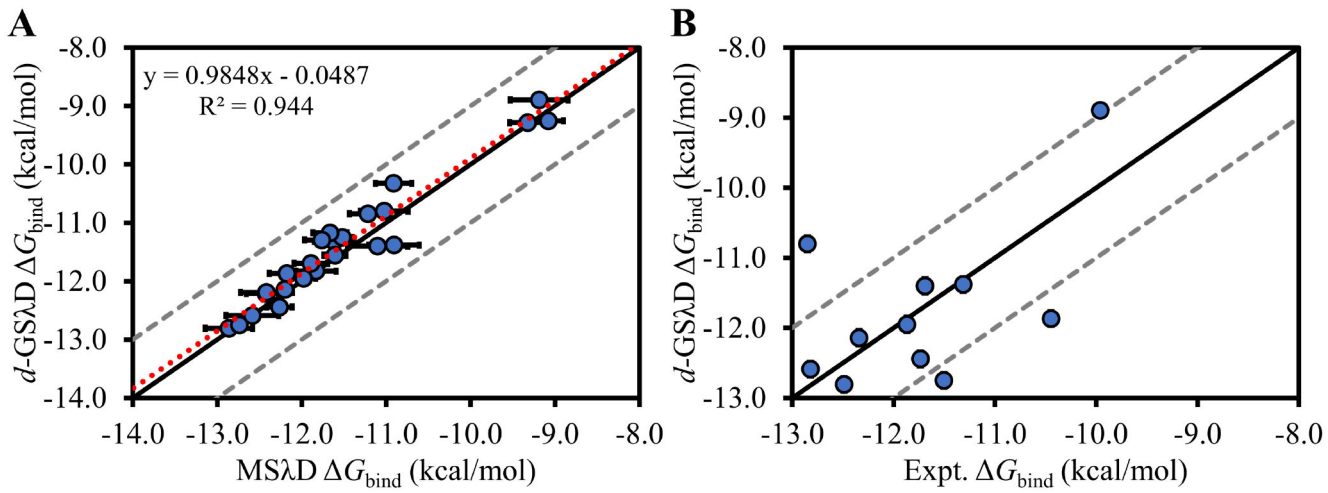

Figure 5.

(A) Correlation between d-GSλD and MSλD for computed binding free energies for indolizine containing catechol diether inhibitors bound to HIV-RT. (B) Correlation in computed *d*-GSλD and experimental binding free energies (kcal/mol). The solid black line represents y = x; dashed grey lines represent y = x ± 1. The red dotted line represents the best fit line of the data.

Table 1.

Computed Free Energy Differences in Water for Two Symmetric Methyl Perturbations Determined with *d*-GSλD (kcal/mol).[a]

Site 1 (X)	Site 2 (Y)	$\Delta G_{water} \pm \sigma$
	Toluene → Toluene	
CH_3 (A)	H	0.000 ± 0.000
CH_3 (B)	H	0.004 ± 0.020
	p-Xylene → p-Xylene	
CH_3 (A)	CH_3 (C)	0.000 ± 0.000
CH_3 (A)	CH_3 (D)	−0.019 ± 0.017
CH_3 (B)	CH_3 (C)	−0.010 ± 0.016
CH_3 (B)	CH_3 (D)	−0.019 ± 0.023

[a]Pairs of symmetric but distinct CH3 groups are labeled A, B and C, D.